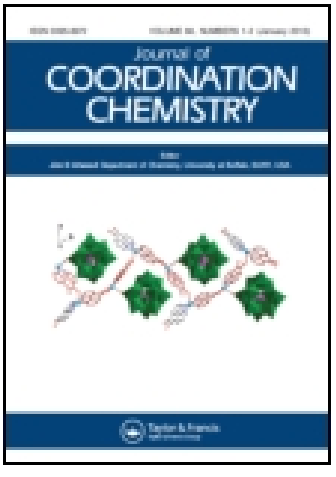

Journal of Coordination Chemistry
Publication details, including instructions for authors and subscription information:
http://www.tandfonline.com/loi/gcoo20

Analysis of vibrational spectra (FT-IR and VCD) and nonlinear optical properties of $[Ru(L)_3]^{2+}$ complexes

Nasarul Islam[a] & Altaf Hussain Pandith[a]
[a] Department of Chemistry, University of Kashmir, Srinagar, India
Accepted author version posted online: 04 Sep 2014.Published online: 07 Oct 2014.

To cite this article: Nasarul Islam & Altaf Hussain Pandith (2014) Analysis of vibrational spectra (FT-IR and VCD) and nonlinear optical properties of $[Ru(L)_3]^{2+}$ complexes, Journal of Coordination Chemistry, 67:20, 3288-3310, DOI: 10.1080/00958972.2014.961921

To link to this article: http://dx.doi.org/10.1080/00958972.2014.961921

Journal of Coordination Chemistry, 2014
Vol. 67, No. 20, 3288–3310, http://dx.doi.org/10.1080/00958972.2014.961921

Analysis of vibrational spectra (FT-IR and VCD) and nonlinear optical properties of $[Ru(L)_3]^{2+}$ complexes

NASARUL ISLAM and ALTAF HUSSAIN PANDITH*

Department of Chemistry, University of Kashmir, Srinagar, India

(*Received 5 March 2014; accepted 16 August 2014*)

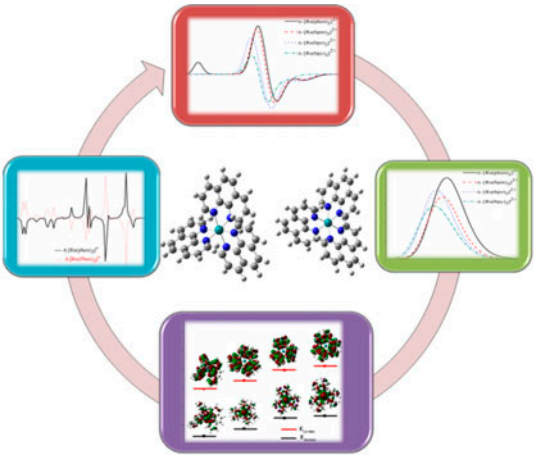

Density functional theory calculations were performed on $[Ru(L)_3]^{2+}$ (L = 1,10-phenanthroline, 2,2′-bipyridine, 2,2′-bipyrimidine, 2,2′-bipyrazine) complexes by employing B3PW91 functional and LAN2DZ basis set to predict their spectra and nonlinear optical response. The geometrical and coordination energy studies explained that the stability of $[Ru(L)_3]^{2+}$ metal complexes depends on the extent of interaction of the dπ orbitals of Ru^{2+} with the π* ligand orbitals, which is maximum for 1,10-phenanthroline. The two enantiomers of the $[Ru(L)_3]^{2+}$ show IR absorption peaks in the region of 1100–1800 cm^{-1}, and a slight shift occurs to lower frequency by solvent. The vibrational circular dichroism peaks of $[Ru(phen)_3]^{2+}$ had major contribution from out-of-phase stretching of 1,10-phenanthroline rings and a minor contribution from H–C=C–H wagging and C=C stretching of rings. Maximum hyperpolarizability was observed for $[Ru(phen)_3]^{2+}$ due to stronger anharmonicity in the π-electron system. Among the $[Ru(L)_3]^{2+}$ (L = bpy, bpm, and bpz) complexes, $[Ru(bpm)_3]^{2+}$ shows enhanced hyperpolarizability due to increase in the dipole along the *X*-direction. In derivative Ru^{2+} complexes, we found that hyperpolarizability depends on electron-donating capability of the substituent. As per FMOs study, the HOMO is predominantly metal fragment based, the LUMO is primarily ligand based, and the larger value of hyperpolarizability corresponds to the lower E_{LUMO}–E_{HOMO} gap, reflecting that nonlinear optical response is a consequence of additive dipolar responses of charge transfer and hyperpolarizability.

Keywords: Ruthenium; Density function theory; Coordination energy; Enantiomers; Hyperpolarizability

*Corresponding author. Email: altafpandit23@gmail.com

1. Introduction

Due to their rich photochemistry and photosensitizing applications, d^6 coordination complexes having nitrogen heterocyclic ligands, such as 1,10-phenanthroline (phen), 2,2′-bipyridine (bpy), 2,2′-bipyrimidine (bpm), 2,2′-bipyrazine (bpz) and their derivatives, have received much attention during the last two decades. Ruthenium complexes with organic ligands, in particular, possess long-lived metal-to-ligand charge transfer (MLCT) excited states and exhibit interesting properties having applications in electrochemistry, photoluminescence, solar energy conversion, dye-sensitized solar cells (DSSCs), sensors and nonlinear optics [1–10]. According to Kinnunen *et al.* [11], electrochemical applications of bipyridine/pyridine-substituted ruthenium systems are based on the relatively low MLCT energy, which mainly involves electron transfer from metal d-orbitals to ligand π^*-orbitals. Ru(II) complexes $[RuL_3]^{2+}$ (L being nitrogen containing ligands) possess sufficiently high thermal and chemical stability and are mostly studied due to their rich photophysical and redox properties [12, 13]. Because of their chemical stability, facile electron transfer, strong luminescence emission, and relatively long-lived excited states [14, 15], such compounds have potential applications in nonradioactive DNA probes or therapeutic agents [16–23] and molecular recognition [24–27]. This class of compounds has been incorporated in solar energy-harvesting devices. The discovery of the optoelectronic properties of $[Ru(bpy)_3]^{2+}$ [28, 29] has stimulated research, where a landmark was the development of DSSCs by Gratzel and co-workers with a ruthenium(II)-coordination compound (molecular sensitizer or dye) constituting the most critical part of the cell [30]. Ru(II) polypyridine complexes $[RuL_3]^{2+}$ have attracted attention in connection with the development of artificial multicomponent systems for photoinduced electron or energy transfer and other related photonic devices [31]. The $[Ru(\mathbf{L})_3]^{2+}$-type complexes have distorted octahedral geometry with D_3 symmetry, **L** being noncylindrical bidentate ligands (see figure 1), and exist in two enantiomeric forms, Δ and Λ.

Recently, quantum chemical computations on transition metal complexes, applying the Density functional theory (DFT) method, have been reported [32–44]. According to Amer *et al.* [15], electronic properties of $[Ru(\mathbf{L})_3]^{2+}$ complexes can be effectively manipulated by ligand exchange or modification. It has been reported that the variation of the ligand sphere can induce changes in the electron distribution around the metal center and, in turn, modify the photochemical properties of the complexes [45]. Density functional MO (molecular orbital) calculations for stacked DNA base pairs using $[Ru(\mathbf{L})_3]^{2+}$ backbones were reported by Kurita and Kobayashi [46]. Ziegler *et al.* calculated electronic structures and circular dichroism spectra of bpy and phen complexes of iron(II) using the TD-DFT method [47]. Zheng *et al.* reported studies on disubstitution effects, electron structures, and related properties in some Ru(II) polypyridyl complexes using DFT [48]. These theoretical studies at electronic structures level aimed at elucidation of the structural properties, and structure-activity relationships of such complexes are very significant in guiding experimental work. Structural, spectral, and chiroptical properties of a number of chiral $[M(L)_3]^{n+}$ complexes have been investigated by several workers, employing quantum chemical computations [34, 49].

Vibrational circular dichroism (VCD) measures the differential absorption of left *versus* right circularly polarized IR light during molecular vibrational excitations. VCD is a valuable technique for determining the solution conformation of chiral transition-metal complexes [49]. The unique nature of VCD spectroscopy results from the combination of a number of vibrational transitions spanning the (3N-6) vibrational modes of a chiral

molecule, N, being the number of atoms in the molecule [50]. Extending the application of *ab initio* analysis, computationally, VCD and IR band assignments in the gas and liquid phases were evaluated for a large number for transition metal complexes [39–44, 51–53].

The work reported here was carried in two parts. In first part, we simulated infrared (IR) and VCD spectra of $[Ru(phen)_3]^{2+}$, $[Ru(bpy)_3]^{2+}$, $[Ru(bpm)_3]^{2+}$, and $[Ru(bpz)_3]^{2+}$ complexes in different solvents, on their optimized molecular structures, using DFT. In the second part, we calculated nonlinear optical properties of these complexes and their derivatives.

2. Computational details

The quantum chemical computations on Ru^{2+} complexes were performed using the Gaussian 03 quantum chemistry package [54]. The initial geometries were optimized by the DFT method by employing Becke's three-parameter hybrid functional B3PW91 and LAN2DZ basis set [55, 56]. That the optimized structures are real energetic minima was established by getting positive values for all the frequencies on the potential energy surface. IR and VCD spectra of two enantiomeric forms (Δ and Λ) were calculated at the same level of theory. The VCD intensities were calculated with the magnetic field perturbation method [57] implemented in the Gaussian 03 set of codes, using Gage Invariant Atomic Orbitals. In order to obtain real-time spectral frequencies, all the calculated frequencies were uniformly scaled by 0.97 for all the conformers. The excited state characteristic excitation energy (in nm) and oscillator strength of the ultraviolet and circular dichroism spectral peaks were calculated using TD-DFT approach [58], employing B3PW91 exchange correlation functional and LAN2DZ basis set on initially optimized geometries of neutral molecules in gas phase and ethanol solution. The polarizable continuum model (IEFPCM) was used for modeling the effects of solvent on the molecular properties of complexes [59]. The total dipole moment (μ), average linear polarizability (α), and first-order hyperpolarizability (β) were calculated from Gaussian 03 W output files using equations (1)–(3) [60].

$$\mu = (\mu_x^2 + \mu_y^2 + \mu_z^2) \tag{1}$$

$$\alpha = \frac{1}{3}(\alpha_{xx} + \alpha_{yy} + \alpha_{zz}) \tag{2}$$

$$\beta = [(\beta_{xxx} + \beta_{xyy} + \beta_{xzz})^2 + (\beta_{yyy} + \beta_{yzz} + \beta_{yxx})^2 + (\beta_{zzz} + \beta_{zxy} + \beta_{zyy})^2]^{\frac{1}{2}} \tag{3}$$

The B3PW91 functional was chosen based on numerous earlier studies which suggest it to be efficient and reasonably accurate in predicting ground and excited state energies of a broad range of organic molecules and inorganic complexes [38, 42, 43, 61, 62].

3. Results and discussion

3.1. *Molecular geometry*

The optimized structures of all the studied compounds with atom numbering scheme are shown in figure 2. Some selected structural parameters (bond lengths and angles) of the four

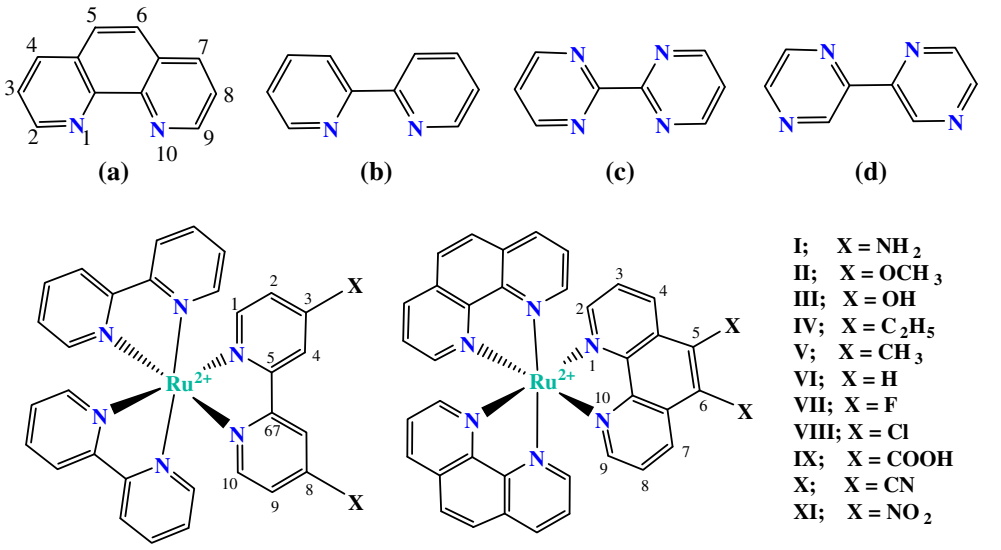

Figure 1. Sketches of the ligand structures (a) 1,10-phenanthroline, (b) 2,2′-bypridine, (c) 2,2′-bipyrimidine, and (d) 2,2′-bipyrazine and derivatives of Ru(II) complexes.

$[Ru(\mathbf{L})_3]^{2+}$ complexes are listed in table S1 (see online supplemental material at http://dx.doi.org/10.1080/00958972.2014.961921), along with their corresponding experimental data [34, 63] and root mean square error. From a comparison between optimized and experimental parameters, we find that the optimized bond lengths and bond angles of optimized structures are closer to experimental ones, agreeing within a range of 0.05–0.09 Å and 0.5°–1.0°, respectively. The negligible differences in the structural parameters may be ascribed to the fact that the experimental values are for crystalline molecular aggregates having intermolecular interaction, whereas theoretical studies are calculated for gas-phase isolated molecule. The Cartesian coordinates of all the calculated optimized geometries are given in table S2 (Supplementary material). From table S1, it is clear that the Ru–N bond distances increase in the sequence Ru–N(bpz) (2.1035 Å) < Ru–N(bpm) (2.1041 Å) < Ru–N(bpy) (2.1095 Å), as expected on the basis of the π-back bonding interaction between the dπ orbitals of ruthenium(II) and the π^* ligand orbitals of different ligands. For example, the Ru–N distance is shorter in the case of $[Ru(phen)_3]^{2+}$ complexes than in $[Ru(bpy)_3]^{2+}$ derivatives, phen being a better π acceptor than bpy. In order to discuss theoretically the coordination stabilities of the complexes, we calculated their coordination energy (ΔE) [64] and free energy change (ΔG) using equations (4) and (5). Further, change in free energy was correlated with log K using equation (6),

$$\Delta E = E_{\mathrm{Ru}}^{2+} + 3E\mathrm{L} - E_{\mathrm{complex}} \tag{4}$$

where E_{Ru}^{2+}, E_{L}, and E_{complex} are the energies of metal ion, ligand, and the complex, respectively (L = bpy, bpm, bpz, phen)

$$\Delta G_{\mathrm{complex}} = G_{\mathrm{complex}} - (G_{\mathrm{Ru}}^{2+} + 3G_{\mathrm{L}}) \tag{5}$$

Table 1. Computed values of SPE (a.u.), coordination energy (ΔE_{water}), free energy change (ΔG), and stability constants (log K) calculated at B3PW91/LAN2DZ level of theory.

	SPE (gas)	SPE (ethanol)	SPE (water)	SPE (acetonitrile)	ΔE (water)	ΔG (water)	Log K
$[Ru(phen)_3]^{2+}$	−1787.3793	−1787.5628	−1787.5706	−1787.5654	1.1888	2907.917	3.861697
$[Ru(bpy)_3]^{2+}$	−1561.4663	−1561.6568	−1561.6647	−1561.6594	1.1737	2890.432	3.213631
$[Ru(bpm)_3]^{2+}$	−1656.0827	−1656.2976	−1656.3022	−1656.3004	1.1102	2724.968	3.175763
$[Ru(bpz)_3]^{2+}$	−1656.0365	−1656.2650	−1656.2775	−1656.0365	1.0486	2562.609	3.148258
Ru(II)	−92.7127	−93.4621	−93.4840	−93.4725			
Phen	−564.4959	−564.5080	−564.5087	−564.5080			
Bpy	−489.1933	−489.2051	−489.2058	−489.2050			
Bpm	−520.7533	−520.7682	−520.7690	−520.7684			
Bpz	−520.7584	−520.7682	−520.7690	−520.7586			

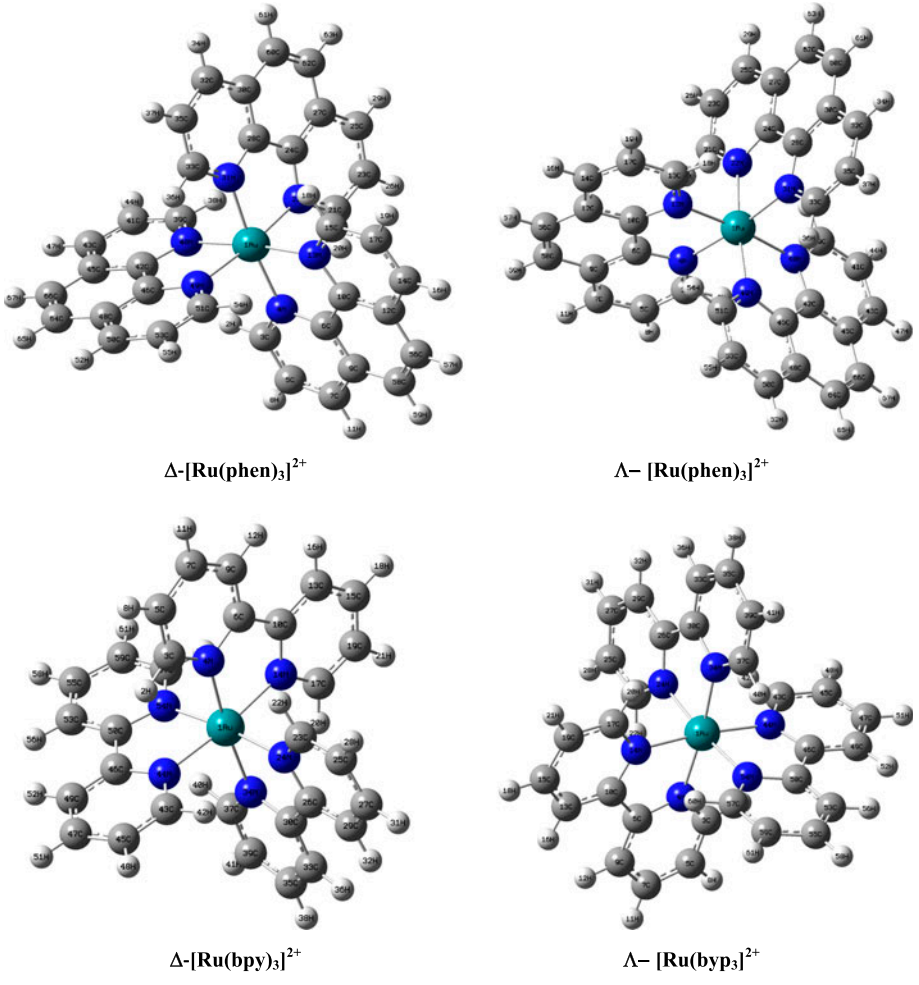

Figure 2. Optimized geometry of the Δ and Λ enantiomers of $[Ru(phen)_3]^{2+}$, $[Ru(bpy)_3]^{2+}$, $[Ru(bpm)_3]^{2+}$ and $[Ru(bpz)_3]^{2+}$.

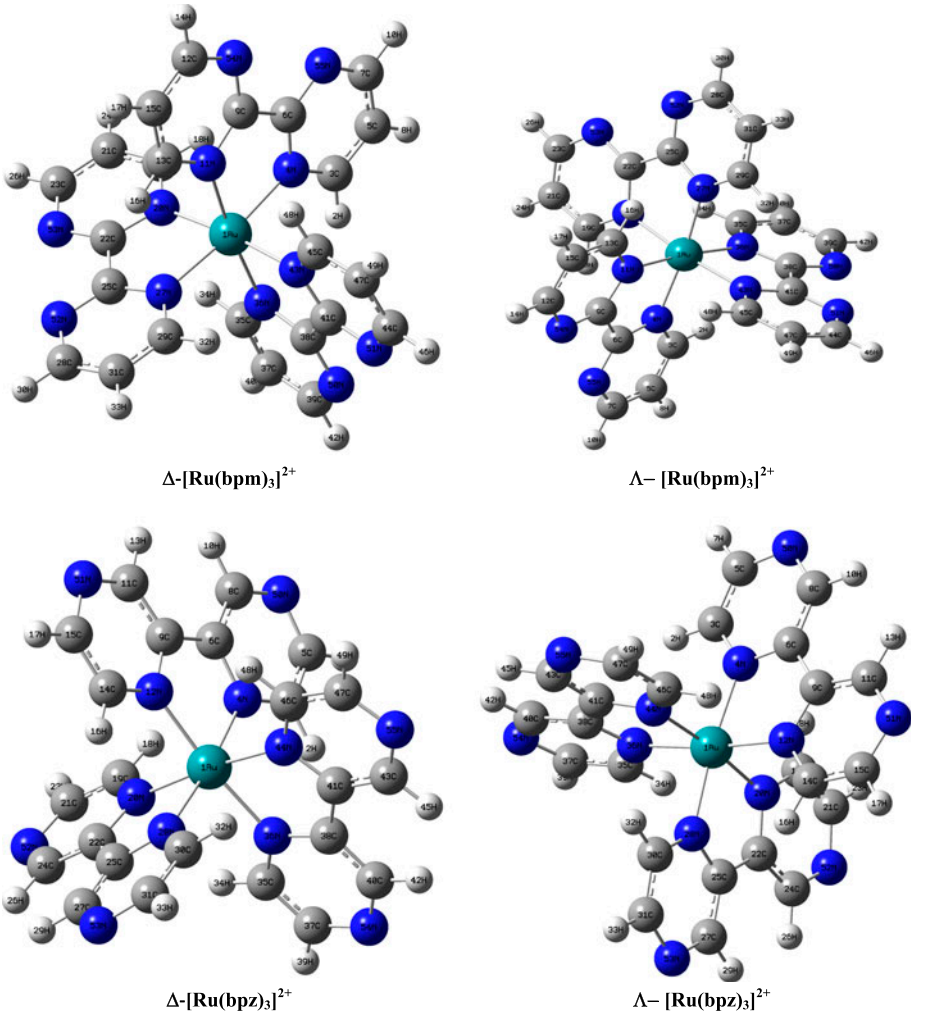

Figure 2. (*Continued*).

where G_{Ru}^{2+}, G_L, and $G_{complex}$ are the free energies of metal ion, ligand, and the complex, respectively.

$$\text{Log}\, K = -\Delta G_{complex}/2.303\, RT \tag{6}$$

Theoretically computed values of single-point energy (SPE), coordination energy, free energy change (ΔG), and stability constants (log K) for the studied complexes are reported in table 1. From the values of their single-point energies, the ruthenium complexes are more solvated in water as compared with acetonitrile and ethanol and the solvation energies parallel the polarity of the solvents. The coordination energy of complexes in water are $[Ru(phen)_3]^{2+}$ (1.1888) > $[Ru(bpy)_3]^{2+}$ (1.1737) > $[Ru(bpm)_3]^{2+}$ (1.1102) > $[Ru(bpz)_3]^{2+}$ (1.0486). According to equation (4), the larger positive value of ΔE, and hence the greater the algebraic value of the coordination energy, reflects greater stability of the complex. This

indicates that Ru^{2+} forms more stable complex with phen than other ligands studied in this work and the trend of their coordination stabilities follows the order $[Ru(phen)_3]^{2+} > [Ru(bpy)_3]^{2+} > [Ru(bpm)_3]^{2+} > [Ru(bpz)_3]^{2+}$. This stability order is also reflected from the order of theoretically calculated stability constant (log *K*). The trend is consistent with the order of the π-acid character of the studied ligands, being maximum for 1,10-phenanthroline.

3.2. *Vibrational analysis*

We have calculated the normal modes of vibration for both enantiomers of the Ru^{2+} complexes under investigation. The two enantiomers, Δ and Λ, of these Ru^{2+} complexes show no significant dissimilarities in the IR absorptions, but their VCD spectra have enantiomer-specific features and can be used for the determination of the absolute configuration of the particular enantiomer. There is slight shift in frequency to lower values by employing polar (water) or less polar (ethanol or acetonitrile) solvent, reflecting the stability of Ru^{2+} complexes in polar solvents. Some selected simulated vibrational frequencies of the $[Ru(phen)_3]^{2+}$ and $[Ru(bpy)_3]^{2+}$ complexes are compared with the experimental values, along with proper assignments, in table S3 (see Supplementary material). The infrared spectrum obtained for Ru^{2+} complexes displays characteristic peaks in the mid-IR regions 1100–1800 cm^{-1}. For $[Ru(phen)_3]^{2+}$ (see figure 3), the IR absorption in mid-IR region are at 1172, 1358, 1400, 1436, 1451, 1481, 1511, 1637, and 1684 cm^{-1}. These vibrations have major contribution from out-of-phase stretching of 1,10-phenanthroline rings and a minor contribution from H–C=C–H wagging and C=C stretching of rings. An additional IR band appears at 3481 cm^{-1} corresponding to C–H stretch of 1,10-phenanthroline rings. Excitation of Ru–C bond occurs at lower frequency, 765 cm^{-1}. Figure 3 shows a remarkable solvent effect. The IR bands have low intensity in solvent phases as compared with gaseous phase and shift to lower frequencies, which may be attributed to the intermolecular interaction occurring in solution. The vibrational frequencies observed for $[Ru(L_3)]^{2+}$, where L = bpy, bpm, and bpz, arise exclusively in the ligand part of the complex. IR spectra of three complexes are remarkably similar except peak intensity. However, an additional peak appears in the bmp complex at 1611 cm^{-1} [see figure 4 and figure S1 (Supplementary material)]. The characteristic IR bands of $[Ru(L_3)]^{2+}$ at 1278, 1323, 1365, 1446, 1489, 1610, and 1696 cm^{-1} are assigned to out-of-phase stretching of the aromatic rings and C=C stretching. An additional IR band at 3489 cm^{-1} is attributed to terminal C–H stretch. Simulated IR peaks for $[Ru(bpy)_3]^{2+}$ and $[Ru(phen_3)]^{2+}$ are in agreement with the experimental data (see table S3, Supplementary material).

VCD spectra show a strong dependence on the configuration of ligands around the metal complex, as expected for such systems. The VCD signal of $[Ru(phen)_3]^{2+}$ due to out-of-phase stretching modes of three 1,10-phenanthroline rings displays two doublets at 1139, 1154, 1267, and 1305 cm^{-1}, respectively [see figure 5(a)], which show right (negative) polarization for Δ-configuration and left (positive) polarization for Λ-configuration without changing the sign of polarization. VCD signals for Δ and Λ configurations show opposite polarization at 1480, 1586, and 1693 cm^{-1} with enhanced intensity, and change the sign of polarization at the two frequencies (1520 and 1632 cm^{-1}). The enhanced polarization may be due to the combined effect of out-of-phase stretching and C=C stretching of 1,10-phenanthroline rings. VCD spectra for C–H stretch of Ru(II) phen complex display negative polarization for Δ-configuration at 3440 and 3480 cm^{-1} and positive polarization for

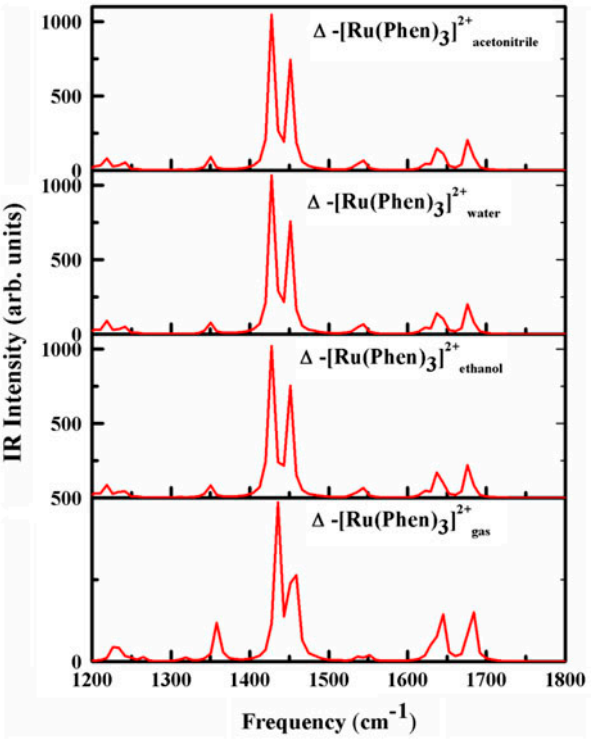

Figure 3. IR spectral intensity in the mid-IR region (1200–1800 cm^{-1}) of $[Ru(phen)_3]^{2+}$ in vacuum, ethanol, water, and acetonitrile; a scale factor of 0.97 is used.

Λ-configuration. In solution [figure 5(b)], there is an overall decrease in the intensity of the VCD signals, most prominent at 1693 cm^{-1}.

The simulated VCD spectra of $[Ru(bpy)_3]^{2+}$ [see figure 6(a)] show a net negative polarization (low intensity) at 1278 and 1701 cm^{-1} with gradual increase in intensity at 1520 and 1549 cm^{-1} for the Δ-configuration (opposite to Λ-configuration), and exhibit a prominent change in polarization at 1521 and 1531 cm^{-1}. These signals arise due to out-of-phase stretch as well as bending of bipyridine rings. An additional peak has been observed with negative polarization of Δ-configuration at 3485 cm^{-1} due to C–H stretch. The peak position does not seem to show any solvent dependence; however, the intensity of peaks is affected by changing the solvent, particularly from 1500 to 1600 cm^{-1} [see figure 6(b)], which may be attributed to intermolecular interaction arising from solvent effects. The trend in the VCD spectra of Δ-$[Ru(bpm)_3]^{2+}$ and Λ-$[Ru(bpm)_3]^{2+}$ (see figure S2) at 1194, 1417, 1418, 1464, and 1491 cm^{-1} matches the pattern of VCD spectra of Δ-$[Ru(bpz)_3]^{2+}$ and Λ-$[Ru(bpz)_3]^{2+}$ [see figure S3 (Supplementary material)], respectively, except in the enhancement of intensity for the latter two enantiomers. However, the VCD bands at 1163 and 1607 cm^{-1} show opposite polarization for Δ-$[Ru(bpm)_3]^{2+}$ and Δ-$[Ru(bpz)_3]^{2+}$; Δ-$[Ru(bpm)_3]^{2+}$ (Λ-$[Ru(bpm)_3]^{2+}$) shows positive (negative) polarization, while Δ-$[Ru(bpz)_3]^{2+}$ (Λ-$[Ru(bpz)_3]^{2+}$) shows negative (positive) polarization. In both $[Ru(bpm)_3]^{2+}$ and $[Ru(bpz)_3]^{2+}$, the Δ-enantiomers are right polarized at 1119, 1194, 1417, and 1491 cm^{-1} and left polarized at 1418 and 1464 cm^{-1}, while the sign of polarization at these frequencies

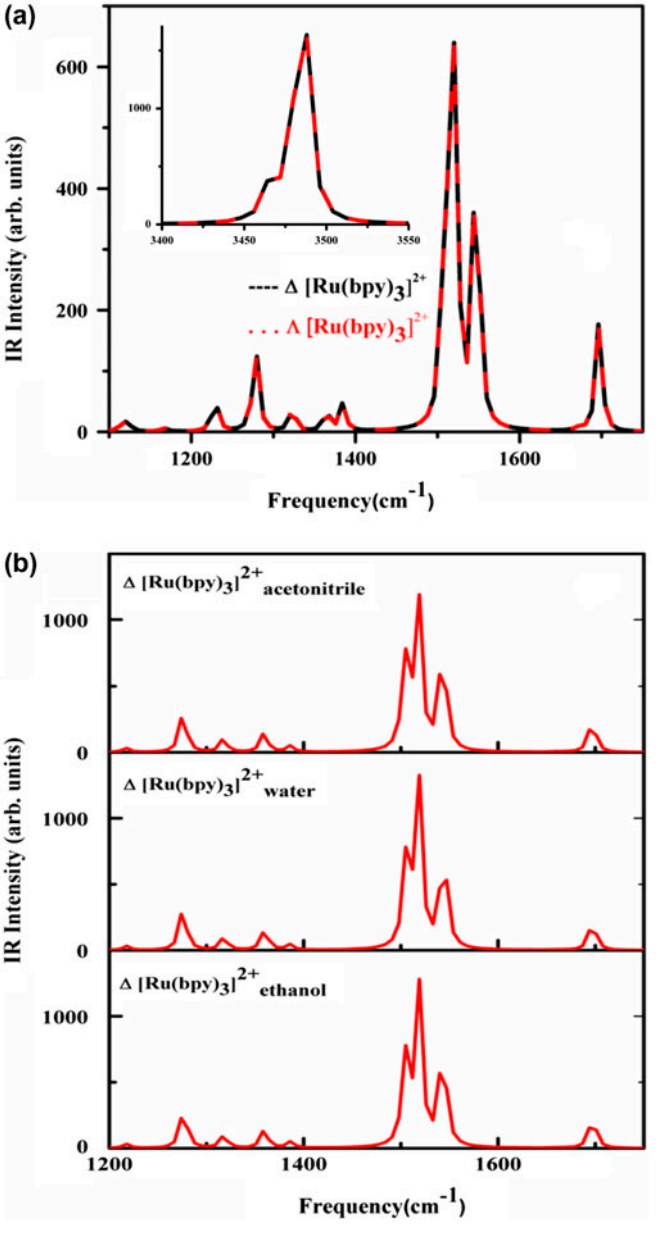

Figure 4. IR spectral intensity in the mid-IR region (1200–1800 cm^{-1}) of $[Ru(bpy)_3]^{2+}$ (a) in vacuum and (b) ethanol, water, and acetonitrile; a scale factor of 0.97 is used.

is opposite for Λ-enantiomers. These VCD bands, which arise due to out-of-phase stretching normal modes of ligand, provide a clear resolution of the configurations of these chiral ruthenium metal complexes. The VCD single pattern at these frequencies does not show any significant change upon solvation, except for peak intensity, with maximum decrease in intensity at 1464 cm^{-1}.

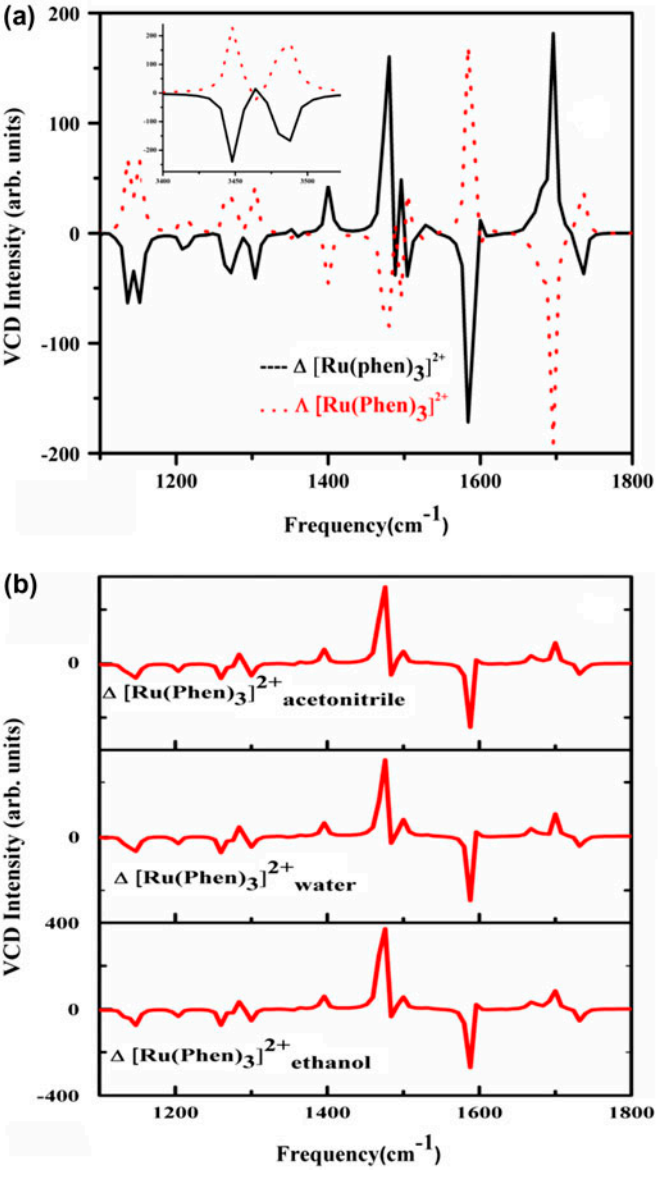

Figure 5. VCD spectral intensity in the mid-IR region (1100–1800 cm^{-1}) of $[Ru(phen)_3]^{2+}$ (a) in vacuum and (b) ethanol, water and acetonitrile; a scale factor of 0.97 is used.

In order to understand the electronic absorption behavior, we employed TD-DFT/LAN2DZ level of theory using the Gaussian 03 package for simulation of electronic absorption spectra in gas phase and in ethanol. For investigating solvation effect on absorption behavior, we adopted the dielectric polarizable continuum model (IEFPCM), which incorporates continuum as polarizable dielectrics. The calculated excitation energies, oscillator strength, and orbital contributions for $[Ru(L)_3]^{2+}$ complexes are shown in table 2.

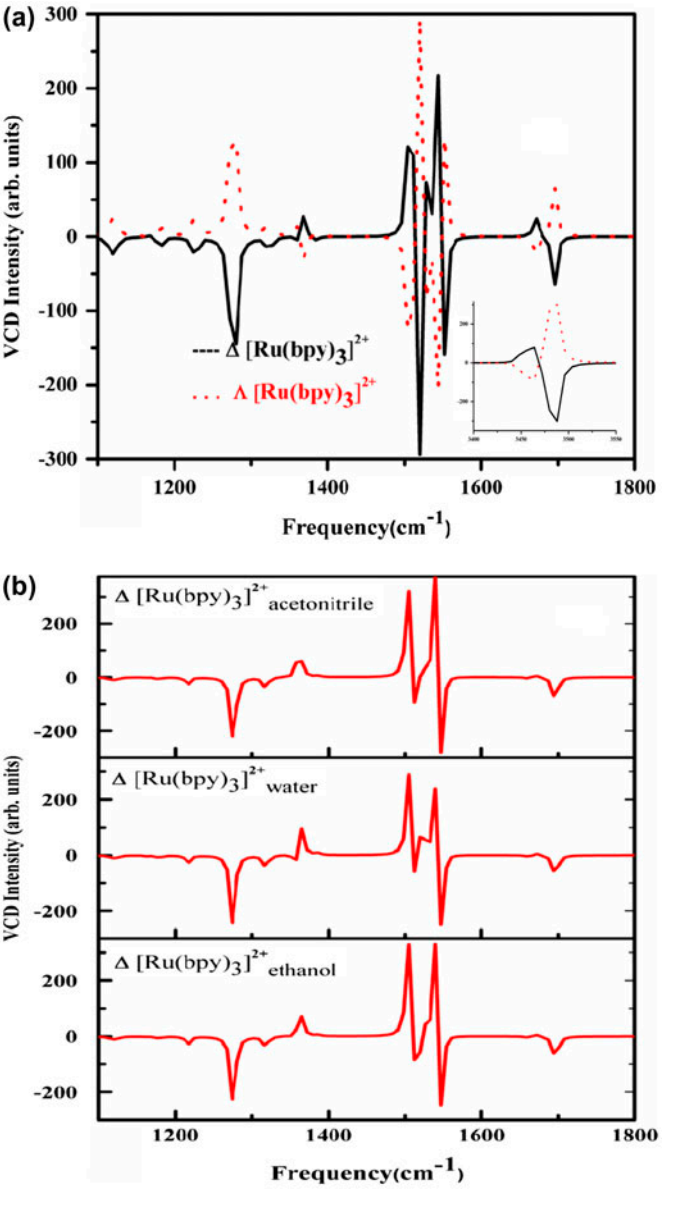

Figure 6. VCD spectral intensity in the mid-IR region (1100–1800 cm^{-1}) of $[Ru(bpy)_3]^{2+}$ (a) in vacuum and (b) ethanol, water, and acetonitrile; a scale factor of 0.97 is used.

$[Ru(phen)_3]^{2+}$ shows a maximum absorption at 362 nm, whereas $[Ru(bpy)_3]^{2+}$, $[Ru(bpm)_3]^{2+}$, and $[Ru(bpz)_3]^{2+}$ show maxima at 356, 361, and 356 nm, respectively. These lowest energy excitations involve charge transfer from filled π-orbital of Ru(II) to π^*-orbital of bidentate ligands (phen, bpy, bpm, and bpz). The simulated spectra in ethanol are consistent with those recorded experimentally [65] see figure 7(a) and (b). The bathochromic shift observed in the solvent phase is due to enhanced stability of the polar excited states of the

metal complexes. The red shift in the UV spectra of $[Ru(phen)_3]^{2+}$ as compared with $[Ru(bpy)_3]^{2+}$, $[Ru(bpm)_3]^{2+}$ and $[Ru(bpz)_3]^{2+}$ is attributed to extended π-conjugation and increased donor properties of 1,10-phenenthroline, whereas in $[Ru(bpm)_3]^{2+}$, the solvato-chromic shift seems primarily due to the increased polar nature of the first excited state [23].

The simulated ECD spectrum of $[Ru(phen)_3]^{2+}$ displays a high-amplitude negative band at 384 nm, an intense positive band at 362 nm, and another low-amplitude band with positive Cotton effect (CE) at 291 nm [see figure 8(a) and (b)]. CD spectra of $[Ru(bpy)_3]^{2+}$, $[Ru(bpm)_3]^{2+}$, and $[Ru(bpz)_3]^{2+}$ display intense negative bands at 373, 378, and 381 nm, respectively, with positive Cotton effect, followed by a high-amplitude positive band (positive CE) at 356, 361, and 356 nm. Theoretically, ECD spectra of Ru(II) complexes exhibit a substantial increase in the Cotton effect of the lowest transition, demonstrating the impact of the addition of extended π-conjugation in case of $[Ru(phen)_3]^{2+}$.

3.3. *Nonlinear optics*

Organometallic and coordination complexes have emerged as chromophores for producing NLO materials, due to the large variety of structures and diversity of electronic properties that are possible by virtue of tunable metal centers [66]. These compounds have the combined properties of both organic and inorganic compounds. The metal centers usually form π bonds with ligands and with each other, resulting in charge-transfer transitions, i.e. ligand to metal, metal to ligand, etc. Photophysical investigation of Ru^{2+} complexes containing polypyridine ligands as well as their nonmetallated counterparts has been reported since the 1990s by groups such as Wang and Wasielewski, Yellowless *et al.*, as well as the Schanze group [67]. The above-mentioned Ru^{2+} complexes possess D_3 symmetry and are octapolar metal complexes [68]. Their relatively high NLO responses are attributed to intense multidirectional [$d\pi(Ru^{2+}) - \pi^*$ (bpy or phen)] MLCT (metal ligand charge transfer) excitations. Electronic descriptors such as polarizabilities (α) and hyperpolarizabilities (β) of such chemical systems characterize their response to an applied electric field. These quantities (α and β) determine the strength of molecular interactions as well as the cross section of different scatterings and collisions. Thus, optical nonlinearity in these complexes is likely a consequence of additive dipolar responses of MLCT, α, and β. The calculated values of electronic parameters such as dipole moment, polarizability, and hyperpolarizability obtained using equations (1)–(3) for these complexes are given in table 2. The values of polarizability and hyperpolarizability reveal that these complexes are good candidates for NLO properties. Among these complexes, the $[Ru(phen_3)]^{2+}$ has maximum hyperpolarizability, possibly due to stronger anharmonicity and extension of the π-electron system. A comparison between these $[Ru(L_3)]^{2+}$ (L = bpy, bpm, and bpz) complexes show enhancement of nonlinearity for $[Ru(bpm_3)]^{2+}$, due to increase in the dipole along the *X*-direction, resulting in more polarizations along this direction. The substitution effect on nonlinear properties of Ru^{2+} complexes was investigated using different electron-donating and withdrawing groups as substituents on bpy and phen backbones (see figure 1). From table 3, it is clear that the substituents have slight effects on geometrical parameters of these complexes. The π-electron-withdrawing substituents decrease the Ru–N bond length and increase the N–Ru–N angle, whereas electron-donating groups have an opposite effect; although the overall substitution effect on geometrical parameters of the complexes are negligible.

Table 2. Key transitions, transition energy (cm^{-1}), wavelength (λ nm), oscillator strengths (f), and orbital contribution for $[Ru(L)_3]^{2+}$ metal complexes calculated at TD-DFT level of theory.

	$[Ru(phen)_3]^{2+}$					$[Ru(bpy)_3]^{2+}$			
	Energy	λ	f	Contribution		Energy	λ	f	Contribution
1	24288.75	411.71	0.001	HOMO->LUMO (98%)	1	24539.59	407.50	0.002	HOMO->LUMO (98%)
2	24804.14	403.16	0.001	HOMO->L + 1 (94%)	2	25183.22	397.09	0.003	HOMO->L + 1 (95%)
3	24821.88	402.87	0.003	HOMO->L + 2 (94%)	3	25197.74	396.86	0.001	HOMO->L + 2 (95%)
4	25322.89	384.90	0.030	H-2->LUMO (11%), H-1->LUMO (70%)	4	26551.15	373.63	0.020	H-1->LUMO (78%), H-2->LUMO (5%)
5	26344.67	379.58	0.030	H-2->LUMO (70%), H-1->LUMO (11%)	5	26568.09	376.39	0.019	H-2->LUMO (78%), H-2->L + 1 (7%)
6	26518.08	377.10	0.003	H-2->L + 1 (27%), H-1->L + 2 (25%)	6	26823.77	372.80	0.001	H-2->L + 2 (48%), H-1->L + 1 (47%)
7	27671.46	362.38	0.217	H-2->L + 1 (38%), H-1->L + 2 (37%)	7	28191.69	354.71	0.120	H-2->L + 1 (22%), H-2->L + 2 (18%)
8	27681.14	361.26	0.217	H-2->L + 2 (38%), H-1->L + 1 (38%)	8	28205.40	355.54	0.122	H-2->LUMO (10%), H-2->L + 2 (23%)
9	29137.79	343.20	0.003	H-2->L + 1 (17%), H-2->L + 2 (22%)	9	29883.05	334.64	0.001	H-2->L + 1 (30%), H-1->L + 2 (31%)
10	34277.99	291.73	0.134	HOMO->L + 3 (43%), H-2->LUMO (4%)	10	30321.01	329.80	0.000	H-3->LUMO (49%), H-8->L + 1 (8%)
	$[Ru(bpm)_3]^{2+}$					**$[Ru(bpz)_3]^{2+}$**			
1	25443.74	393.02	0.001	HOMO->LUMO (98%)	1	24007.40	414.25	0.002	HOMO->LUMO (98%)
2	26044.63	383.96	0.003	HOMO->L + 1 (68%), HOMO->L + 2 (23%)	2	25131.60	397.91	0.001	HOMO->L + 1 (96%)
3	26050.27	383.87	0.003	HOMO->L + 1 (23%), HOMO->L + 2 (68%)	3	25147.73	397.65	0.003	HOMO->L + 2 (96%)
4	26149.59	381.06	0.027	H-2->LUMO (36%), H-1->LUMO (50%)	4	26394.70	377.01	0.024	H-1->LUMO (79%), H-1->L + 1 (8%)
5	26368.14	370.81	0.022	H-2->LUMO (49%), H-1->LUMO (36%)	5	26597.12	375.98	0.024	H-2->LUMO (79%), H-1->L + 2 (7%)
6	27277.86	366.60	0.000	H-2->L + 2 (29%), H-1->L + 1 (30%)	6	26781.82	373.39	0.000	H-2->L + 2 (48%), H-1->L + 1 (47%)
7	27488.43	361.57	0.122	H-2->L + 2 (27%), HOMO->L + 3 (34%)	7	27964.24	357.60	0.138	H-2->L + 2 (33%), H-1->LUMO (13%)
8	27894.07	358.50	0.092	H-1->L + 2 (27%), HOMO->L + 4 (34%)	8	27965.85	356.58	0.139	H-2->LUMO (13%), H-2->L + 1 (33%)
9	27951.34	357.76	0.001	H-2->L + 1 (12%), HOMO->L + 5 (69%)	9	29943.54	333.96	0.001	H-2->L + 1 (37%), H-1->L + 2 (38%)
10	28792.58	347.31	0.001	H-2->L + 10 (11%), H-1->L + 9 (12%)	10	30939.64	323.21	0.001	H-5->L + 1 (15%), H-3->LUMO (54%)

Interestingly, the Ru–N bond lengths and N–Ru–N bond angles for remaining unsubstituted ligand show opposite change upon substitution. The coordination energies of $[Ru(bpy)_2(bpy)']^{2+}$ derivatives [where (bpy)′ represents ligand with substituents] are 0.781(**1**) > 0.778(**2**) > 0.773(**3**) > 0.769(**4**) > 0.763(**5**) > 0.761(**6**) > 0.758(**7**) > 0.752(**8**) > 0.768(**9**) > 0.763(**10**) > 0.761(**11**) > 0.753(**12**) and of $[Ru(phen_2)(phen)']^{2+}$ derivatives are 0.948(**1**) > 0.935(**2**) > 0.933(**3**) > 0.901(**4**) > 0.889(**5**) > 0.887(**6**) > 0.881(7) > 0.88 (**8**) > 0.878(**9**) > 0.875(**10**) > 0.871(**11**) > 0.867 (12), respectively. Ru^{2+} complexes of bpy derivatives are less stable than Ru^{2+} complexes of phen derivatives; however, within the same group (i.e. either bpy derivatives or phen derivatives), the stronger the

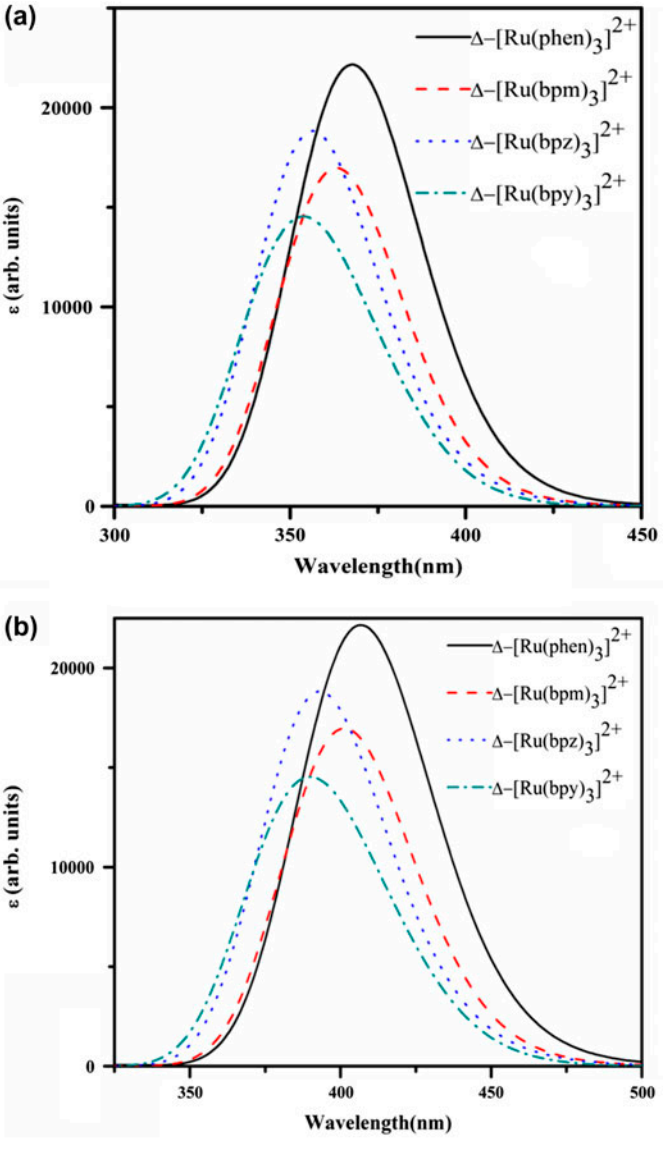

Figure 7. UV–Visible spectra of $[Ru(L)_3]^{2+}$ (a) in vacuum and (b) ethanol; a scale factor of 0.97 is used.

electron-donating ability of the substituent, the higher the stability of the Ru^{2+} octahedral complexes with bidentate ligands. From table 4, it is evident that the magnitude of the hyperpolarizability of all $[Ru(phen)_3]^{2+}$ and $[Ru(bpy)_3]^{2+}$ derivatives is significantly affected by incorporation of substituent on phen or bpy backbone. The values of hyperpolarizability depend on the electron-donating capability of substituent; the metal complex (I) with NH_2 as the donor group gives a higher value for hyperpolarizability as compared with complex (V) where the donor group is CH_3. The enhancement of first hyperpolarizability from VI to I is attributed to enhanced electron density to

Table 3. Computed values of polarizability ($\alpha \times 10^{-24}$ esu), dipole moment (μ, debye), and hyperpolarizability ($\beta \times 10^{-30}$ esu) for $[Ru(phen)_3]^{2+}$, $[Ru(bpy)_3]^{2+}$, $[Ru(bpm)_3]^{2+}$, and $[Ru(bpz)_3]^{2+}$ calculated at B3PW91/LAN2DZ level of theory.

	$[Ru(phen)_3]^{2+}$				$[Ru(bpy)_3]^{2+}$			
Property	Gas	Ethanol	Water	Acetonitrile	Gas	Ethanol	Water	Acetonitrile
α_{xx}	55.74568	73.293	59.62817	55.68308	46.29677	46.31083	46.34516	46.3903
α_{xy}	−0.04061	0.0206	0.015561	−0.01853	−0.01482	−0.00104	−0.00089	0.009929
α_{yy}	55.37893	73.16856	57.38649	55.34277	46.14533	46.25974	46.07731	46.09998
α_{xz}	−0.06165	0.067431	0.015709	−0.08981	−0.02712	0.003112	−0.04135	−0.05424
α_{yz}	−0.11486	0.047128	−0.09085	−0.07706	0.039421	−0.03097	−0.08922	−0.06995
α_{zz}	49.72451	69.85866	49.72317	49.74704	43.18652	42.98912	43.09449	43.06396
α_{total}	53.64148	72.13976	58.60434	53.61604	45.23039	45.20742	45.19319	45.20564
μ_x	−1.8194	−2.3913	−1.7724	−1.829	−1.5011	−1.4923	−1.5153	−1.5062
μ_y	0.02	0.0235	0.0025	0.0331	−0.0042	0.0007	0.0082	0.0007
μ_z	−0.0354	0.0328	−0.0261	0.0295	0.0023	0.0148	−0.016	0.0373
μ_{total}	1.8199	2.3917	1.7726	1.8296	1.5011	1.4924	1.5154	1.5067
β_{xxx}	5286.8	8441.2	−9836.96	7155.725	−5055.93	−5825.53	5377.3	4877.367
β_{xxy}	−4630	−11,820	−1989.69	−5760.87	−2943.66	−574.753	−2312	−3219.21
β_{xyy}	−5288	−8346	6802.77	−4147.4	5077.2	5829.588	−5404	−4919.34
β_{yyy}	4601.8	11,801	6969.214	5732.977	2973.777	573.9616	2325.8	3254.57
β_{xxz}	−12.86	7.1008	−16.0375	39.082513	−1.89191	9.819045	−17.67	10.43111
β_{xyz}	−15.39	−5.824	5.984115	−7.39797	−17.8412	6.152382	−19.53	−29.0313
β_{yyz}	3.551	−2.291	50.568864	9.517335	−0.77866	1.774166	−17.22	15.19583
β_{xzz}	8.215	−12.5	−3.72587	71.53102	−26.8002	−3.33952	29.209	33.85466
β_{yzz}	−1.71	11.805	1.262473	−2.88621	−25.2309	2.453551	2.0584	−19.5018
β_{zzz}	−3.224	6.6492	−3.75345	6.862734	1.816628	6.361078	−13.46	28.2037
β_{total}	39.92942	82.61975	342.78014	236.64191	18.35184	14.40209	52.63151	22.89005
		$[Ru(bpm)_3]^{2+}$				**$[Ru(bpz)_3]^{2+}$**		
α_{xx}	44.13819	57.03994	58.23593	57.38552	43.15014	56.53319	57.50259	43.15014
α_{xy}	0.004891	−0.01304	0.113521	0.007114	−0.00163	−0.01571	−0.03705	−0.00163
α_{yy}	44.02459	56.70888	57.92575	57.2095	43.07433	56.28725	57.36155	43.07433
α_{xz}	−0.0329	−0.07143	0.012597	−0.0532	−0.01941	−0.09648	−0.0243	−0.01941
α_{yz}	−0.03498	0.093662	−0.14346	−0.05528	−0.03423	−0.06788	−0.0621	−0.03423
α_{zz}	41.31179	55.20198	56.8676	55.1264	41.76765	56.33304	57.28819	41.76765
α_{total}	43.17807	56.34263	57.70266	56.59965	42.68348	56.40996	57.41001	42.68348
μ_x	−0.0012	−1.848	1.8997	−1.8724	−1.4032	−0.0009	−1.8337	−1.4032
μ_y	0.0032	0.012	−0.0533	0.0078	0.0079	−0.0133	0.06	0.0079

μ_z	0.0012	0.0134	0.0213	−0.0015	μ_z	0.0033	0.0015	−0.0136	0.0033
μ_{total}	0.0036	1.8481	1.9005	1.8724	μ_{total}	1.4033	0.0134	1.8348	1.4033
β_{xxx}	3045.2	−6680	8529.731	6443.283	β_{xxx}	4674.8	6248.6	10676.82	4674.847
β_{xxy}	−2797	−5701	−4722.88	−5933.19	β_{xxy}	−3277	−10,604	−7475.27	−3276.87
β_{xyy}	−3061	6740.6	−8367.31	−6491.71	β_{xyy}	−4689	−6306	−10690.4	−4688.99
β_{yyy}	2793.5	5767.1	4641.473	5888.457	β_{yyy}	3281.7	10,591	7443.102	3281.656
β_{xxz}	−10.68	20.618	−115.117	−21.0387	β_{xxz}	−2.841	1.5678	16.41816	−2.84101
β_{xyz}	8.9213	−24.58	−37.321	21.84138	β_{xyz}	−1.944	−44.98	7.653627	−1.94356
β_{yyz}	8.8276	−15.88	50.04471	36.41136	β_{yyz}	5.4253	10.658	48.33899	5.425254
β_{xzz}	23.409	−49.93	121.7634	55.82518	β_{xzz}	17.413	23.842	34.62762	17.41319
β_{yzz}	−26.71	−52.86	−91.0325	−76.1571	β_{yzz}	−11.49	−0.621	−53.4261	−11.4874
β_{zzz}	1.0778	1.1364	−22.2036	20.03943	β_{zzz}	1.0614	−5.076	36.58965	1.061429
β_{total}	36.61377	42.72155	332.5458	144.2207	β_{total}	8.73172	53.68929	127.8399	8.73172

π-conjugation. Bpy and phen are π-electron-rich systems; when acceptor groups like NO_2 are attached to them, the donor ability of the ligand gets reduced and, hence, leads to a reduction in β value. Thus, in metal complexes VII–XII, the hyperpolarizabilities decrease with increase in electron-withdrawing nature of attached group.

To understand this phenomenon in the context of molecular orbitals, we examined the HOMO and LUMO states generated via GAUSSIAN03W using TDDFT level of theory. The FMOs of $[Ru(phen)_3]^{2+}$, $[Ru(bpy)_3]^{2+}$, $[Ru(bpm)_3)]^{2+}$, and $[Ru(bpz)_3)]^{2+}$ reveal that the HOMO is predominantly metal fragment based and the LUMO is localized on the ligand (see figure 9). The results (table 5) show that the larger value of first hyperpolarizability correlates to lower E_{LUMO}–E_{HOMO} gap, reflecting that hyperpolarizability of these metal complexes is caused by charge-transfer characteristics of FMOs. The HOMO of these complexes is mainly dπ-type orbitals, thus highly sensitive to substituent properties. With an increase in π electron-withdrawing ability of the substituent, the Coulombic attraction of the substituent for the electrons on HOMO orbitals is strengthened, resulting in decrease in energy of the molecular HOMO as well as LUMO energy of VII–XII $[Ru(phen)_3]^{2+}$ and $[Ru(bpy)_3]^{2+}$ derivatives. Table 5 shows that increase in β is related to HOMO's energy; generally, higher the HOMO, larger the hyperpolarizability. Thus, strong donating groups lead to higher β values, as for NH_2 – as substituent, due to enhanced metal to ligand charge-transfer transition. Energy gaps are reduced when the two hydrogens are substituted by electron-donating groups, resulting in red shift in electronic absorptions of derivative complexes showing existence of correlation between HOMO and LUMO gaps and β values: the lower is the gap, the higher is the hyperpolarizability of the derivative complex. In this study, we have observed that incorporating the donor groups into metal complexes not only enhances β values, but also decreases the E_{LUMO}–E_{HOMO} gap, as compared with unsubstituted complexes and those with electron-withdrawing substituents. This suggests that the charge-transfer process increases by introducing donor groups in these complexes. In addition to this, we present the effect of substitution on geometrical parameters and coordination stability of metal complexes.

Table 4. Computational results for the main bond lengths (Å), bond angles (°), and coordination energies (a.u) of $[Ru(byp)_3]^{2+}$ and $[Ru(phen)_3]^{2+}$ derivative complexes.

		$[Ru(bpy)_3]^{2+}$					$[Ru(phen)_3]^{2+}$				
S. No	Group	Ru–N*	Ru–N**	A^*	A^{**}	ΔE_{Gas}	Ru–N*	Ru–N**	A^*	A^{**}	ΔE_{Gas}
I	NH2	2.116	2.104	79.03	78.68	0.781	2.0882	2.0751	80.03	79.68	0.948
II	OCH3	2.113	2.105	79.01	78.7	0.778	2.0878	2.0751	80.01	79.68	0.935
III	OH	2.111	2.105	78.94	78.7	0.773	2.0841	2.0754	79.96	79.71	0.933
IV	C2H5	2.11	2.107	78.83	78.7	0.769	2.0832	2.0754	79.96	79.71	0.901
V	CH3	2.109	2.108	78.79	78.71	0.763	2.0798	2.0757	79.8	79.73	0.889
VI	H	2.109	2.109	78.75	78.71	0.761	2.0761	2.0761	79.72	79.75	0.887
VII	F	2.097	2.111	78.04	78.71	0.758	2.0758	2.079	79.69	79.77	0.881
VIII	Cl	2.095	2.111	78.01	78.71	0.752	2.0758	2.079	79.68	79.77	0.880
IX	Br	2.088	2.117	77.97	78.71	0.768	2.0749	2.0822	79.65	79.79	0.878
X	COOH	2.087	2.119	77.97	78.71	0.763	2.0747	2.0831	79.65	79.81	0.875
XI	CN	2.085	2.119	77.95	78.72	0.761	2.0746	2.0854	79.63	79.81	0.871
XII	NO2	2.079	2.121	77.93	78.72	0.753	2.0741	2.0891	79.61	79.83	0.867

*Express coordination length and angle between center ion and ligand with substituents.
**Expresses the co-ligand.

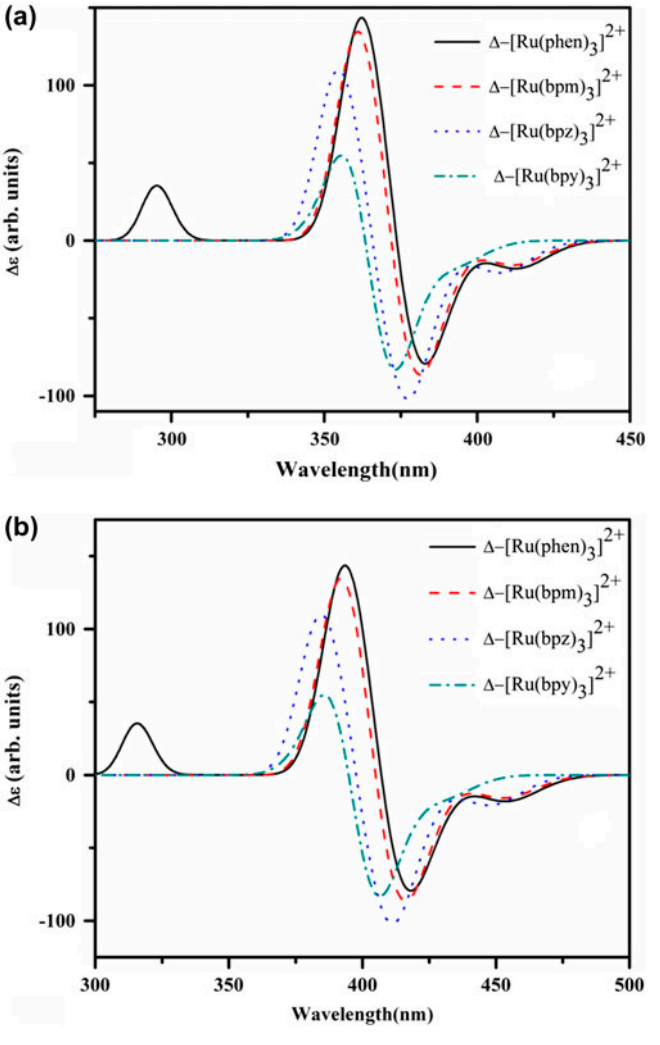

Figure 8. Circular dichroism spectra of $[Ru(L)_3]^{2+}$ (a) in vacuum and (b) ethanol; a scale factor of 0.97 is used.

3.4. *Electrochemical data*

Geometry optimizations of the neutral and oxidized derivative of $[Ru(phen)_3]^{2+}$ and $[Ru(bpy)_3]^{2+}$ were carried out in gas phase and in acetonitrile. The ground-state oxidation potentials were computed from the free-energy differences between the neutral and oxidized ground species and calculated as $(G^0 - G^+)_{GS}$ [69] and are given in table 5. The Gibbs free energy in acetonitrile of the complex (G^c_{act}) is defined as $(G^c_{act}) = G^c_{vac} + \Delta G^c_{act}$, where G^c_{vac} is the Gibbs free energy in gas phase and ΔG^c_{act} is the free energy of solvation. G^c_{vac} is obtained by performing a single-point calculation at the optimized geometry *in vacuo*, followed by frequency calculations in order to include the vibrational contribution to the total partition function. ΔG^c_{act} is obtained by a single-point calculation in a solution and a reference calculation in a gas phase at the geometry optimized in ethanol. The theoretically

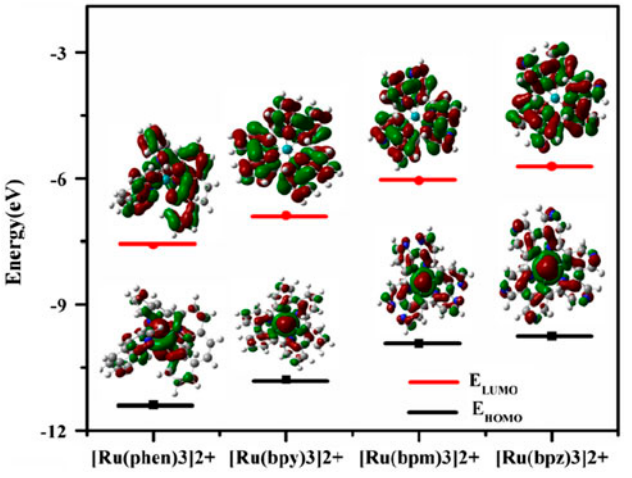

Figure 9. Schematic representation of the energies of HOMO and LUMO molecular orbitals and their related energies for $[Ru(phen)_3]^{2+}$, $[Ru(bpy)_3]^{2+}$, $[Ru(bpm)_3]^{2+}$, and $[Ru(bpz)_3]^{2+}$.

calculated oxidation potential of $[Ru(phen)_3]^{2+}$ and $[Ru(bpy)_3]^{2+}$ are in close agreement with the experimentally calculated values [23, 48]. The results show that the oxidation potentials of $[Ru(phen)_3]^{2+}$ and $[Ru(bpy)_3]^{2+}$ derivatives with electron-donating substituents

Table 5. Computed values of HOMO (eV), LUMO (eV), hyperpolarizabilty ($\beta \times 10^{-30}$ esu), and oxidation potential (eV) of metal complexes at B3PW91/LAN2DZ level of theory.

Complex	Group	E_{HOMO} (eV)	E_{LUMO} (eV)	$\Delta E_{LUMO-HOMO}$	β_{total}	E_{oxd}
$[Ru(bpy)_3]^{2+}$						
I	NH_2	−10.397	−6.69687	3.700832	27.178	1.301
II	OCH_3	−10.547	−6.72681	3.820565	24.356	1.298
III	OH	−10.615	−6.73497	3.880431	23.454	1.297
IV	C_2H_5	−10.620	−6.77307	3.847777	21.645	1.296
V	CH_3	−10.7705	−6.87103	3.89948	20.987	1.296
VI	H	−10.7836	−6.88409	3.89948	18.351	1.295
VII	F	−10.8603	−6.88491	3.975401	18.399	1.293
VIII	Cl	−10.893	−6.89987	3.993089	18.217	1.296
IX	Br	−11.0372	−6.90314	4.134047	18.093	1.296
X	COOH	−11.1515	−6.90858	4.242895	18.013	1.289
XII	CN	−11.1869	−6.90885	4.277999	17.987	1.287
XIII	NO_2	−11.3637	−6.90994	4.453788	17.954	1.285
$[Ru(phen)_3]^{2+}$						
I	NH_2	−10.8875	−7.80195	3.085569	45.675	1.342
II	OCH_3	−11.0943	−7.75841	3.335919	43.786	1.339
III	OH	−11.1515	−7.71025	3.441231	43.778	1.337
IV	C_2H_5	−11.1651	−7.67406	3.491027	41.096	1.337
V	CH_3	−11.3501	−7.61446	3.735663	41.063	1.335
VI	H	−11.3814	−7.55652	3.824919	39.929	1.331
VII	F	−11.4263	−7.55163	3.874717	39.903	1.329
VIII	Cl	−11.4345	−7.53812	3.896486	38.796	1.330
IX	Br	−11.4399	−7.53691	3.903017	38.487	1.328
X	COOH	−11.4753	−7.53473	3.940572	38.084	1.325
XII	CN	−11.5134	−7.53337	3.980027	37.385	1.300
XIII	NO_2	−11.5624	−7.52711	4.035267	37.079	1.298
$[Ru(bpm)_3]^{2+}$	H	−9.92831	−6.05494	3.873356	36.613	1.289
$[Ru(bpz)_3]^{2+}$	H	−9.74271	−5.71751	4.025199	8.7317	1.283

are more positive and those with electron-withdrawing substituents are slightly negative to those of the parent Ru(II) complexes. Thus, ligands with electron-donating substituents are stronger π-acceptors than the ligand (phen or bpy) in the parent complexes. In all the derivative complexes modeled here, the first reduction is consistent with the addition of electrons to the LUMO localized on ligand [23]. Thus, the oxidation center is localized on the Ru(II) and the first reduction center is localized on the ligand; efficiency of this process increases with increase in electron-donating character of substituents present on the ligand. Therefore, the above theoretical data will be helpful in developing highly stable metal complexes with strong nonlinear optical responses.

4. Conclusion

We carried out theoretical studies on Ru^{2+} complexes by employing DFT at B3PW91/LAN2DZ level. The geometrical parameters of optimized metal complexes were in agreement with experimental parameters; the bond lengths agreeing within 0.05–0.09 Å and the bond angles agreeing within 0.5°–1°. Ru–N bond distances increase in the sequence Ru–N (bpz) < Ru-N(bpm) < Ru-N(bpy) as expected on the basis of dπ–π* orbital interactions as compared with $[Ru(Phen)_3]^{2+}$, the better π acceptor. We observed that the coordination energy of Ru^{2+} complexes in water follows the trend $[Ru(\mathbf{phen})_3]^{2+}$ (1.1888) > $[Ru(\mathbf{bpy})_3]^{2+}$ (1.1737) > $[Ru(\mathbf{bpm})_3]^{2+}$ (1.1102) > $[Ru(\mathbf{bpz})_3]^{2+}$ (1.0486) reflecting the stability of $[Ru(\mathbf{phen})_3]^{2+}$. The IR spectrum obtained for Ru^{2+} complexes displays characteristic peaks from 1100 to 1800 cm^{-1}. For $[Ru(\mathbf{phen})_3]^{2+}$, the out-of-phase stretching of 1,10-phenthroline rings, H–C=C–H wagging, and C=C stretching of rings contribute to IR and VCD spectra. Due to the intermolecular interaction occurring in solution, the IR bands have low intensity in solution compared with gaseous phases. The vibrational frequencies observed for $[Ru(L)_3]^{2+}$, where L = bpy, bpm, and bpz, arise exclusively in the ligand part of complex. The *ab initio* predicted frequencies for $[Ru(\mathbf{bpy})_3]^{2+}$ and $[Ru(\mathbf{phen})_3]^{2+}$ are in fair agreement with the experimental ones. The Ru^{2+} complexes show relatively high NLO responses, which may be a consequence of additive dipolar responses of MLCT, α, and β; $[Ru(\mathbf{phen})_3]^{2+}$ has maximum hyperpolarizability. A comparison between different $[Ru(\mathbf{L})_3]^{2+}$ (L = bpy, bpm, and bpz) complexes reveal enhancement of nonlinearity for $[Ru(\mathbf{bpm})_3]^{2+}$, which is due to an increase in dipole moment along the *X*-axis, resulting in more polarization. Substituents have small effects on geometrical parameters and the magnitude of hyperpolarizability mainly depends upon the electron-donating capability of a substituent. The HOMO is predominantly metal localized and the LUMO is primarily ligand centered. A significant correlation exists between E_{LUMO} and E_{HOMO} gap and β values; the lower the gap, the higher the hyperpolarizability of a derivative complex. Oxidation potentials of $[Ru(phen)_3]^{2+}$ and $[Ru(byp)_3]^{2+}$ derivatives with electron-donating substituents are more positive and those with electron-withdrawing substituents are slightly negative to those of parent Ru(II) complexes. These theoretical findings are significant in the sense that these may guide in developing highly stable Ru^{2+} complexes with meaningful nonlinear optical applications.

Supplementary material

Supporting information contains figure S1 [IR spectral intensity in the mid-IR region (1200–1800 cm^{-1}) of (a) $[Ru(bpm)_3]^{2+}$ and (b) $[Ru(bpz)_3]^{2+}$, a scale factor of 0.97 is used], figure S2 [VCD spectral intensity in the mid-IR region (1100–1800 cm^{-1}) of $[Ru(bpm)_3]^{2+}$ (a) in vacuum, and (b) ethanol, water, and acetonitrile, a scale factor of 0.97 is used] and figure S3 (VCD spectral intensity in the mid-IR region (1100–1800 cm^{-1}) of $[Ru(bpz)_3]^{2+}$ (a) in vacuum, and (b) ethanol, water, and acetonitrile, a scale factor of 0.97 is used). Table S1 (optimized and experimental geometrical parameters (bond length and bond angle) of Ru(II) complexes), table S2 (Cartesian coordinates of the ruthenium(II) complexes calculated at B3PW91 /LAN2DZ level of theory) and table S3 [theoretical and experimental IR frequencies of $Ru(phen)_3]^{2+}$ and $[Ru(byp)_3]^{2+}$ complexes].

Acknowledgements

We are thankful to the Head, Department of Chemistry, University of Kashmir, for providing the necessary laboratory facility for carrying out this work. A.H.P thanks the University Grants Commission (UGC), Government of India for research grant [F.No. 42-305/2013 (SR)].

Supplemental data

Supplemental data for this article can be accessed here. http://dx.doi.org/10.1080/00958972.2014.961921.

References

[1] E.A. Seddon, K.R. Seddon. *The Chemistry of Ruthenium*, Elsevier, New York (1984).
[2] M. Venturi, S. Serroni, A. Juris, S. Campagna, V. Balzani. *Top. Curr. Chem.*, **197**, 193 (1998).
[3] L. DeCola, P. Belser. *Coord. Chem. Rev.*, **177**, 30 (1998).
[4] V. Balzani, S. Campagna, G. Denti, A. Juris, S. Serroni, M. Venturi. *Acc. Chem. Res.*, **31**, 26 (1998).
[5] P. Belser, S. Bernhard, C. Blum, A. Beyeler, L. DeCola, V. Balzani. *Coord. Chem. Rev.*, **155**, 190 (1999).
[6] F. Barigelletti, L. Flamigni. *Chem. Soc. Rev.*, **29**, 1 (2000).
[7] K. Kalyanaundram. *Coord. Chem. Rev.*, **46**, 159 (1992).
[8] (a) J. Barber, B. Andersson. *Nature*, **370**, 31 (1994); (b) K.N. Ferreira, T.M. Iverson, K. Maghlaoui, J. Barber, S. Iwata. *Science*, **303**, 1831 (2004).
[9] A. Benniston, A. Harriman, F. Romero, R. Ziezzel. *J. Chem. Soc., Dalton Trans.*, 1233 (2004).
[10] J.G. Vos, J.M. Kelly. *Dalton Trans.*, 41, 4889 (2006).
[11] T.J.J. Kinnunen, M. Haukka, T.A. Pakkanen. *J. Organomet. Chem.*, **654**, 8 (2002).
[12] T. Kennelly, H.D. Gafney, M. Braun. *J. Am. Chem. Soc.*, **107**, 4431 (1985).
[13] S. Zalis, R.F. Winter, W. Kaim. *Coord. Chem. Rev.*, **254**, 1383 (2010).
[14] A. Juris, V. Balzan, F. Barigelletti, S. Campagna, P. Belser, A. Von Zelewsky. *Coord. Chem. Rev.*, **84**, 85 (1988).
[15] A.G. Amer, A.A. Hamid, S. Kanan. *J. Coord. Chem.*, **65**, 420 (2012).
[16] I. Haq, P. Lincoln, D. Suh, B. Norden, B.Z. Chowdhry, J.B. Chaires. *J. Am. Chem. Soc.*, **117**, 4788 (1995).
[17] Z. Ji, S.D. Huang, A.R. Guadalupe. *Inorg. Chim. Acta*, **305**, 127 (2000).
[18] C.J. Murphy, J.K. Barton. *Methods Enzymol.*, **226**, 576 (1993).
[19] C. Moucheron, A.K.-D. Mesmaeker, S. Choua. *Inorg. Chem.*, **36**, 584 (1997).
[20] C.M. Dupureur, J.K. Barton. *Inorg. Chem.*, **36**, 33 (1997).
[21] Y. Jenkins, A.E. Friedman, N.J. Turro, J.K. Barton. *Biochemistry*, **31**, 10809 (1992).
[22] A.E. Friedman, J.-C. Chambron, J.-P. Sauvage, N.J. Turro, J.K. Barton. *J. Am. Chem. Soc.*, **112**, 4960 (1990).

[23] (a) K. Ohkubo, T. Hamada, H. Ishida. *Chem. Commun.*, **18**, 1423 (1993); (b) H. Durr, R. Schwarz, C. Andries, I. Willner. *J. Am. Chem. Soc.*, **115**, 12362 (1993); (c) F. Cheng, J. Chen, F. Wang, N. Tang, L. Chen. *J. Coord. Chem.*, **65**, 205 (2012).
[24] M. Atsumi, L. González, C. Daniel. *J. Photochem. Photobiol. A*, **190**, 310 (2007).
[25] V.W.-W. Yam, V.W.-M. Lee. *Inorg. Chem.*, **36**, 2124 (1997).
[26] P.D. Beer, N.C. Fletcher, T. Wear. *Polyhedron*, **15**, 1339 (1996).
[27] P.D. Beer, F. Szemes. *Chem. Commun.*, **21**, 2245 (1995).
[28] J.P. Paris, W.W. Brandt. *J. Am. Chem. Soc.*, **81**, 5001 (1959).
[29] A. Philippopoulos, P. Falaras, E. Chatzivasiloglou, O. Markopoulou, V. Likodimos, G.C. Konti. *J. Coord. Chem.*, **65**, 2535 (2012).
[30] (a) M. Gratzel. *Acc. Chem. Res.*, **42**, 1788 (2009); (b) M. Gratzel. *J. Photochem. Photobiol. A*, **164**, 3 (2004).
[31] (a) V. Balzani, A. Juris, M. Venturi, S. Campagna, S. Serroni. *Chem. Rev.*, **96**, 759 (1996); (b) T. Saita, H. Nitadori, A. Inagaki, M. Akita. *J. Organomet. Chem.*, **694**, 3125 (2009).
[32] A. Voigt, U. Abram, R. Bottcher, U. Richter, J. Reinhold, R. Kirmse. *Chem. Phys.*, **253**, 171 (2000).
[33] S. Tobisch, T. Nowak, H. Bögel. *J. Organomet. Chem.*, **619**, 21 (2001).
[34] S.R. Stoyaner, J.M. Villegas, D.P. Rillema. *Inorg. Chem.*, **41**, 2941 (2002).
[35] D.A. Young, E.D. Lipp, L.A. Nafie. *J. Am. Chem. Soc.*, **107**, 6205 (1985).
[36] A. Chaudhari, S.L. Lee. *Int. J. Quantum Chem.*, **107**, 212 (2007).
[37] T.B. Freedman, X. Cao, D.A. Young, D.L. Elmer, L.A. Nafie. *J. Phys. Chem. A*, **106**, 3560 (2002).
[38] N. Norani, H. Rahemi, S.F. Tayyari, M.J. Riley. *J. Mol. Model.*, **15**, 25 (2009).
[39] Y. He, X. Cao, L.A. Nafie, T.B. Freedman. *J. Am. Chem. Soc.*, **123**, 11320 (2001).
[40] (a) H. Sato, T. Taniguchi, K. Monde, S.-I. Nishimura, A. Yamagishi. *Chem. Lett.*, **35**, 364 (2006); (b) H. Sato, K. Taniguchi, A. Nakahashi, K. Monde, A. Yamagishi. *Inorg. Chem.*, **46**, 6755 (2007).
[41] A.H. Pandith, S.K. Pati. *J. Phys. Chem. A*, **114**, 87 (2010).
[42] A.H. Pandith, N. Islam, Z.F. Syed, S. Rehman, S. Bandaru, A. Anoop. *Chem. Phys. Lett.*, **516**, 199 (2011).
[43] H. Sato, Y. Mori, Y. Fukuda, A. Yamagishi. *Inorg. Chem.*, **48**, 4353 (2009).
[44] L.A. Nafie. *J. Phys. Chem. A*, **108**, 7222 (2004).
[45] (a) K. Kalyanasundaram, M. Gratzel (Eds.). *Photosensitization and Photocatalysis Using Inorganic and Organometallic Compounds*, Kluwer Academic Publishers, Dordrecht (1993); (b) T.-J.J. Kinnunen, M. Haukka, M. Nousiainen, A. Patrikka, T.A. Pakkanen. *J. Chem. Soc., Dalton Trans.*, 2649 (2001); (c) C. Sahin, C. Varlikll, C. Zafer, Q. Shi, R.E. Douthwaite. *J. Coord. Chem.*, **66**, 1384 (2013).
[46] N. Kurita, K. Kobayashi. *Comput. Chem.*, **24**, 351 (2000).
[47] T. Ziegler, J. Fan, J. Autschbach. *Inorg. Chem.*, **49**, 1355 (2010).
[48] (a) K.C. Zheng, J.P. Wang, Y. Shen, D.B. Kuang, F.C. Yun. *Acta Chim. Sinica*, **59**, 1283 (2001); (b) K.C. Zheng, J.P. Wang, W.L. Peng, X.W. Liu, F.C. Yun. *J. Phys. Chem. A*, **105**, 10899 (2001); (c) K.C. Zheng, J.P. Wang, X. Liu, Y. Shen, F.C. Yun. *J. Mol. Struct.*, **577**, 95 (2002); (d) K.C. Zheng, X.W. Liu, J.P. Wang, F.C. Yun, L.N. Ji. *J. Mol. Struct.*, **637**, 195 (2003).
[49] M. Rudolph, J. Autschbach. *J. Phys. Chem. A*, **115**, 2635 (2011); (b) J. Autschbach. *Coord. Chem. Rev.*, **251**, 1796 (2007).
[50] K. Nakanishi, N. Berova, R.W. Woody. In *Circular Dichroism: Principles and Applications*, 2nd Edn, Wiley-VCH, New York (2000).
[51] T. Wu, X.-P. Zhang, C.-H. Li, P. Bour, Y.-Z. Li, X.-Z. You. *Chirality*, **24**, 451 (2012).
[52] H. Amouri, M. Gruselle. *Chirality in Transition Metal Chemistry: Molecules, Supramolecular Assemblies and Materials*, Wiley-VCH, Chichester (2008).
[53] G. Longhi, S. Abbate, R. Gangemi, E. Giorgio, C. Rosini. *J. Phys. Chem. A*, **110**, 4958 (2006).
[54] M.J. Frisch, G.W. Trucks, H.B. Schlegel, G.E. Scuseria, M.A. Robb, J.R. Cheeseman, J.A. Montgomery, Jr. T. Vreven, K.N. Kudin, J.C. Bur-ant, J.M. Millam, S.S. Iyengar, J. Tomasi, V. Barone, B. Mennucci, M. Cossi, G. Scalmani, N. Rega, G.A. Petersson, H. Nakatsuji, M. Hada, M. Ehara, K. Toyota, R. Fukuda, J. Hasegawa, M. Ishida, T. Nakajima, Y. Honda, O. Kitao, H. Nakai, M. Klene, X. Li, J.E. Knox, H.P. Hratchian, J.B. Cross, V. Bakken, C. Adamo, J. Jaramillo, R. Gomperts, R.E. Stratmann, O. Yazyev, A.J. Austin, R. Cammi, C. Pomelli, J.W. Ochterski, P.Y. Ayala, K. Morokuma, G.A. Voth, P. Salvador, J.J. Dannenberg, V.G. Zakrzewski, S. Dapprich, A. Daniels, M.C. Strain, O. Farkas, D.K. Malick, A.D. Rabuck, K. Raghavachari, J.B. Foresman, J.V. Ortiz, Q. Cui, A.G. Baboul, S. Clifford, J. Cioslowski, B.B. Stefanov, G. Liu, A. Lia-shenko, P. Piskorz, I. Komaromi, R.L. Martin, D.J. Fox, T. Keith, M.A. Al-Laham, C.Y. Peng, A. Nanayakkara, M. Challacombe, P.M.W. Gill, B. Johnson, W. Chen, M.W. Wong, C. Gonzalez, J.A. Pople. *GAUSSIAN 03 Revision B 03*, Gaussian Inc., Wallingford, CT (2004).
[55] J.P. Perdew, J.A. Chevary, S.H. Vosko, K.A. Jackson, M.R. Pederson, D.J. Singh, C. Fiolhais. *Phys. Rev. B*, **46**, 6671 (1992).
[56] T.H. Dunning, P.J. Hay. In *Modern Theoretical Chemistry*, H.F. Schaefer III (Ed.), Vol. 3, p. 1, Plenum, New York (1976).
[57] P. Stephens. *J. Phys. Chem.*, **89**, 748 (1985).
[58] R. Bauernschmitt, R. Ahlrichs. *Chem. Phys. Lett.*, **256**, 454 (1996).
[59] G. Scalmani, M.J. Frisch. *J. Chem. Phys.*, **132**, 114110 (2010).

[60] (a) R. Zhang, B. Du, G. Sun, Y. Sun. *Spectrochim. Acta, Part A*, **75**, 1115 (2010); (b) D. Sajan, H. Joe, V.S. Jayakumar, J. Zaleski. *J. Mol. Struct.*, **785**, 43 (2006); (c) H. Alyar, Z. Kantarci, M. Bahat, E. Kasap. *J. Mol. Struct.*, **836**, 516 (2007); (d) N. Sundaraganesan, J. Karpagam, S. Sebastian, J.P. Cornard. *Spectrochim. Acta, Part A*, **73**, 11 (2009).
[61] T.B. Freedman, X. Cao, R.K. Dukor, L. Nafie. *Chirality*, **15**, 743 (2003).
[62] N. Islam, S. Niaz, T. Manzoor, A.H. Pandith. *Spectrochim. Acta, Part A*, **131**, 461 (2014).
[63] (a) S. Betanzos-Lara, O. Novakova, R.J. Deeth, A.M. Pizarro, G.J. Clarkson, B. Liskova, V. Brabec, P.J. Sadler, A. Habtemariam. *J. Biol. Inorg. Chem.*, **17**, 1033 (2012); (b) M. Kozlowska, P. Rodziewicz, D. Malgorzata Brus, J. Czyrko, K. Brzezinski. *Acta Cryst.*, **68**, 1570 (2012).
[64] (a) K.C. Zheng, H.Y. Rao, F. He, Z.T. Xu, H.Q. Liu. *Acta Phys.-Chim. Sin.*, **14**, 299 (1998); (b) K.C. Zheng, J.P. Wang, Y. Shen, W.L. Peng, F.C. Yun. *Dalton Trans.*, **1**, 111 (2002).
[65] D.J. Liard, M. Bosby, P. Matousek, M. Towrie, A. Vicek. *J. Phys. Chem. A*, **108**, 2362 (2004).
[66] (a) M.E. Thompson, P.E. Djurovich, S. Barlow, S.R. Marder. *Comprehensive Organometallic Chemistry III*, D. O. Hare (Ed.), Vol. 12, Elsevier, Amsterdam (in press); (b) J.P. Morall, G.T. Dalton, M.G. Humphery, M. Samoe. *Adv. Organomet. Chem.*, **55**, 61 (2008); (c) J. Heck, S. Dabek, T. Meyer-Friedrichsen, H. Wong. *Coord. Chem. Rev.*, **190**, 1217 (1999); (d) S. Di Bella, C. Dragonetti, M. Pizzotti, D. Roberto, F. Tessore. R. Ugo, *Top. Organomet. Chem.*, **28**, 1 (2010); (e) S. Di Bella. *Chem. Soc. Rev.*, **30**, 355 (2001); (f) C.R. Nayara, R. Ravikumar. *J. Coord. Chem.*, **67**, 1 (2014).
[67] (a) G.B. Cunningham, Y. Li, S. Liu, K.S. Schanze. *J. Phys. Chem. B*, **107**, 12569 (2003); (b) B. Wang, M.R. Wasielewski. *J. Am. Chem. Soc.*, **119**, 12 (1997); (c) S. Liu, K.S. Schanze. *Chem. Commun.*, **13**, 1510 (2004).
[68] S.D. Bella. *Chem. Soc. Rev.*, **30**, 355 (2001).
[69] F. De Angelis, S. Fantacci, A. Selloni. *Nanotechnology*, **19**, 424002 (2008).